DESIGN AND DEVELOPMENT OF A HYBRID TERRAIN VEHICLE

Ying FANG[1]

In order to develop a hybrid vehicle suitable for experimental testing, a series hybrid vehicle is developed based on an all-terrain vehicle that runs on gasoline. The throttle valve control, engine start-stop control, and drive circuit are accomplished by utilizing the STM32 single-chip microcomputer as the main controller. Subsequently, the corresponding program is designed in accordance with the hardware. Eventually, the designed vehicle was tested on an actual road. The results indicate that the vehicle's acceleration time from 0 to 40 km/h is 9.8 seconds. This reveals that the designed hybrid vehicle can operate normally and plays a positive part in researching the performance of hybrid vehicles.

Keywords: hybrid vehicle; mechanical design; control system; test.

1. Introduction

With the rapid advancement of the automobile industry [1], issues such as resource scarcity and environmental pollution have become increasingly severe. Consequently, new energy vehicles, particularly hybrid electric vehicles (HEV) that combine the benefits of electric and traditional internal combustion engine vehicles [2-4], have garnered increasing attention.

HEVs encompass traditional internal combustion engine control [5], motor control [6], battery control [7], and control strategy [8,9], all of which require simulation optimization. Considering fuel economy, battery state of charge, and battery lifespan, Yang formulated a multi-agent reinforcement learning (MARL) model by integrating the multi-objective energy management strategy and reinforcement learning (RL). Simulation outcomes demonstrate that the proposed MARL model has advantages in optimizing multiple objectives, enhancing vehicle performance [10]. Wang also proposed an optimal energy-saving strategy for HEVs based on MARL, which minimizes energy consumption while maintaining a safe following distance. Simulation results reveal that this approach can reduce fuel consumption by 15.8% compared to the state-of-the-art hierarchical model predictive control (MPC) strategy [11]. Sun developed an enhanced model predictive control algorithm based on long short-term memory (LSTM-IMPC) for rational management of PHEV energy. Experimental results show that it can save 18.71% fuel consumption compared to the charge depletion-charge maintenance

[1] Lecture, Department of Automobile, Henan Mechanical and Electrical Vocational College, China, e-mail:361545412@qq.com

(CD-CS) rule in real driving cycles, indicating excellent fuel-saving capabilities [12]. The neural network is also an option for energy management. Li develops a data-driven energy cost model and the battery current model respectively through the neural network as the critical model which is used in speed optimization. This approach achieves collaborative optimization of speed and energy management using a layered optimization architecture[13].Tang employs dual deep reinforcement learning methods, Deep Q Network (DQN) and Deep Deterministic Policy Gradient (DDPG), to learn the shift strategy and throttle opening, respectively. This approach achieves multi-objective synchronous control and optimization of the energy management strategy [14].

Based on the foregoing references, it can be inferred that HEVs can achieve notable enhancements in fuel economy through diverse control models, but experimental testing vehicles are necessary for validation. However, testing HEVs using actual vehicles is impractical due to their large size and high cost. Therefore, an HEV was developed based on an existing All Terrain Vehicle (ATV), facilitating research.

2. The structure of the hybrid electric vehicle

The designed HEV is based on an existing ATV, and its parameters are listed in Table 1. The designed HEV is a series type, with the original engine solely responsible for charging the battery, as shown in Fig. 1. The design process includes selecting the motor, battery, reducer, and designing both the hardware and software of the control system. The preliminary design parameters, based on the ATV's specifications, are shown in Table 2.

Table 1

Parameters of the car

Parameter	Value
Full load mass /kg	300
Engine power/kW	6
Transmission efficiency	0.95
Rolling resistance coefficient	0.015
Windward area	0.5
Tire rolling radius/m	0.228
Air drag coefficient	0.35

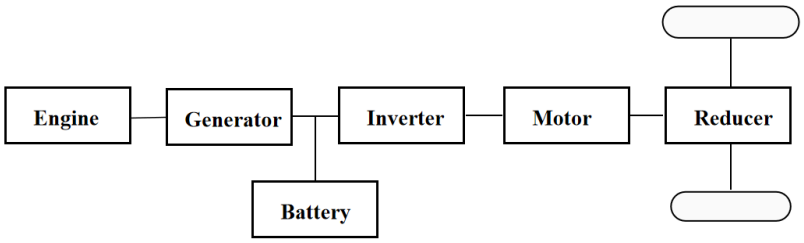

Fig.1 Diagram of the car

Table2

Preliminary design parameter of the car

Index	Value
Maximum speed/km·h^{-1}	50
0-40km/h acceleration time/s	≦10
Maximum climbing degree %	≧30

3. Mechanical design

3.1 Drive motor selection

Currently, drive motors used in HEVs mainly include DC motors, AC induction motors, and permanent magnet synchronous motors, among others. Among these, the permanent magnet synchronous motor is the most suitable option. This is due to its simple structure, high efficiency, and compact size. Additionally, it does not require electronic commutation owing to its permanent magnets. Thus, it is recommended to select this type of motor for optimal performance in terms of maximum speed, acceleration, and maximum climbing capacity.

The power of the motor is calculated based on the following empirical equations, referenced from [15], with the derivations of the equations omitted.

(1) Determine the power of the motor based on the maximum vehicle speed

$$P_m \geq \frac{v_{\max}}{3600\eta}\left(mgf + \frac{C_D A v_{\max}^2}{21.15}\right) \tag{1}$$

where $v_{\max}$ is the maximum vehicle speed, km/h; η is the transmission efficiency; f is the Rolling resistance coefficient; C_D is the Air drag coefficient; A is the Windward area; P_m is the power at the maximum speed, kW.

According to the values in table 1, the calculated power of the motor based on the maximum vehicle speed is 0.95kW.

(2) Determine the power of the motor based on the acceleration performance

$$P_m \geq \frac{v_{\max}}{3600\eta}\left(\frac{\delta m v_e^2}{36dt}\left[1-\left(\frac{t_m - dt}{t_m}\right)^{0.58}\right] + mgfv_e + \frac{C_D A v_e^2}{21.15}\right) \tag{2}$$

where δ is the rotational mass conversion factor of the car and its normal value is 1.1; dt is the iterative step length in the design process and its normal value is 0.1; v_e is the speed at the end of the accelerating process, km/h.

When the speed at the end of the accelerating process is 40km/h,the calculated power of the motor based on acceleration performance is 0.92 kW.

(3)Determine the power of the motor based on the maximum climbing degree

$$P_m \geq \frac{v_{\max}}{3600\eta}(mgf\cos\alpha_{\max} + mg\sin\alpha_{\max} + \frac{C_D A v_i^2}{21.15}) \quad (3)$$

where v_i is the speed during the climbing process, km/h.

If the speed during the climbing process is 5 km/h, the calculated power of the motor based on the maximum climbing degree is 1.3 kW.

Based on the calculation, it can be concluded that the rated power of the drive motor should be at least 0.95kW, while the peak power of the motor should not be less than 1.3kW. After considering the parameters of the ATV and the calculation results, a permanent magnet synchronous motor with a maximum power of 1.5KW and a maximum speed of 5500r/min has been selected. The motor controller has also been chosen according to the selected motor.

3.2 Battery selection

HEVs utilize various types of batteries, including lead-acid, nickel-metal hydride, and lithium-ion batteries. Among these, lithium-ion batteries are favored due to their high energy density and light weight. In electric mode driving, it is crucial that the battery supplies sufficient power to meet the demands of the driving motor and accessories. This can be calculated using formula (4).

$$P_B \geq \frac{P_m}{\eta_B \eta} + \frac{P_a}{\eta_B} \quad (4)$$

where P_B is the peak power of battery, kW; η_B is the battery discharge efficiency; P_m is the peak power of motor, kW; P_a is the power of accessories, kW.

The calculated peak power of the battery is 1.6kW, determined by the motor and accessories of the vehicle.

To ensure that the vehicle can travel the desired distance in electric mode under normal working conditions, the total energy of the battery pack must meet the requirements. The capacity of the battery pack can be calculated using formula (5)[16].

$$W_o \geq \frac{P_B S}{0.7 v_{\max}} \quad (5)$$

where W_o is the capacity of the battery pack, kWh; S is the driving distance at electric mode, km.

According to formula (5), the battery energy is calculated to be 1.83 kWh, given a maximum speed of 50 km/h and a driving distance of 40km.

It is important to ensure that the voltage of the battery pack falls within the appropriate range for the vehicle's power system. This ensures that the battery voltage is compatible with the selected drive motor voltage. The battery capacity can be calculated based on the voltage using formula (6).

$$C_E = \frac{1000 W_o}{U_E} \quad (6)$$

where U_E is the voltage of the battery, V; C_E is the capacity of the battery, Ah.

Based on the available battery resources, the battery pack is composed of 100 individual lithium batteries, each with an operating voltage of 1.2 volts. Fifty of these batteries are connected in series to form a group, and two groups are then connected in parallel. As a result, the total voltage output of the battery pack is 60 volts, and the battery has a capacity of 30.5 Ah. The type is BF60305LV manufactured by the CHILWEE company.

3.3 Reducer

The speed of the drive motor is so high that it cannot directly drive the wheel, therefore, it needs to be reduced through a reducer. Based on the maximum speed of the vehicle and the maximum speed of the drive motor, the minimum transmission ratio can be obtained using formula (7)[16].

$$i \le 0.377 \frac{n_m r}{v_{\max}} \tag{7}$$

where n_m is the motor maximum speed, r/min; r is the radius of the tire, m.

According to the vehicle data and formula (7), the required reduction transfer ratio is 9.45. Therefore, the reducer is selected based on this transfer ratio.

4. Control system hardware design

The control system, also known as the energy management system, regulates the engine to charge the battery. Its primary function is to collect data on battery voltage and current, which is then used to estimate the battery's State of Charge (SOC). Based on this data, it controls the engine's charging by adjusting the throttle valve position and managing the engine start-stop function.

The hardware of the control system can be divided into four parts: data acquisition, main controller, and drive circuits, as depicted in Figure 2. The data acquisition circuit collects battery voltage, battery current, engine speed, and throttle position data using an A/D converter and I/O ports. The main controller processes the collected data to calculate the battery SOC value and then issues command to control the throttle valve position and engine start-stop. The drive circuit controls both the throttle and the engine start-stop functions.

4.1 Main controller

The main controller used in this system is the STM32F103VET6 microcontroller, a 32-bit controller with an internal 72 MHz main frequency, low power consumption, and a 12-channel ADC acquisition peripheral[17].

This peripheral can read analog signals from voltage sensors and current sensors. The microcontroller also features a 7-channel DMA controller that can rapidly transfer data within itself. Additionally, it has two SPI channels that can transmit data between the microcontroller and the LCD display screen. It also

includes eight internal 4-channel TIM timer peripherals for timing interrupt processing.

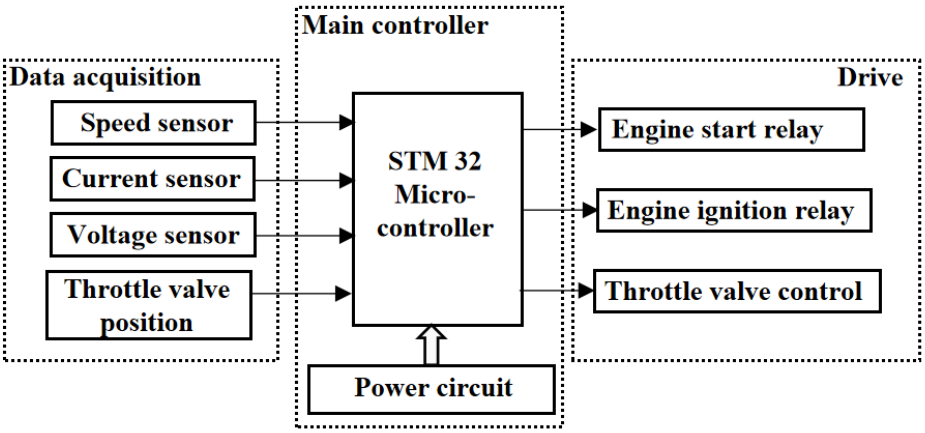

Fig.2 Diagram of the control system hardware

4.2 Power Management Circuit

The control system uses an external 24V DC power supply, directly connected to the voltage and current sensors. However, the servo and display systems require a 5.0V power supply, while the STM32 microcontroller system and speed sensor need a 3.3V power supply. Therefore, DC-DC converter circuits are designed to convert 24V to 5.0V and 5.0V to 3.3V. The 24V to 5.0V circuit uses the XLM2596-5 chip, which supports a maximum input voltage of 36V and a maximum output current of 3A, ensuring stable output. The 5.0V to 3.3V circuit uses the AMS117-3.3 chip. Both circuits are depicted in Figures 3 and 4.

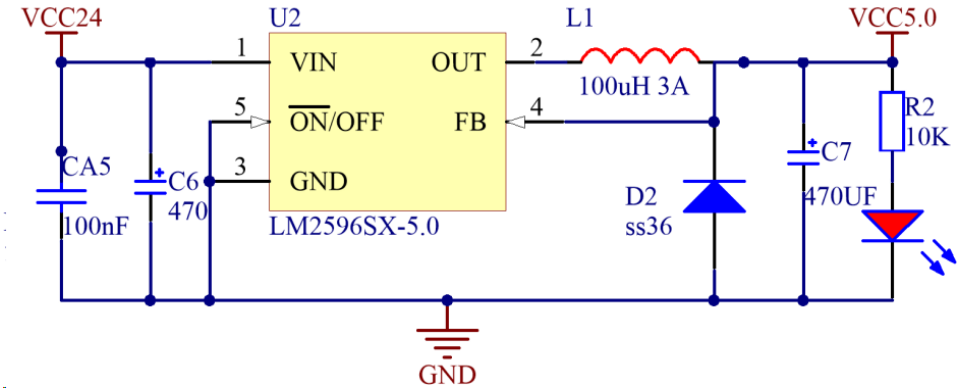

Fig.3 Circuit of LM2596-5.0

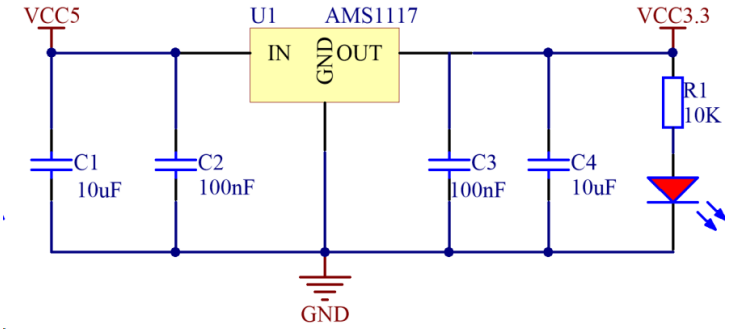

Fig.4 Circuit of AMS117-3.3

4.3 Data Acquisition

Data acquisition is crucial, involving the collection of four essential parameters: battery voltage, battery current, engine speed, and throttle valve position. These parameters are classified as analog and digital data. Battery voltage, battery current, and throttle valve position are analog data, while engine speed is digital data.The ADC port receives analog data, while the I/O port receives digital data.

To input data directly to the microcontroller, the voltage range must be within 0-3.3V. The throttle valve position sensor is a sliding resistance.When the throttle is pressed, the idle signal line is disconnected, the sliding resistance also follows the rotation, and the voltage value changes. So the microcontroller can receive the voltage and detect the value of the throttle valve position opening when the sensor connects to the microcontroller directly and the power supply voltage is 3.3V. For the voltage and current sensor, two converters are utilized. The voltage sensor converts the input range of 0-100V to 0-3.3V, while the current sensor converts the input range of 0-50A to 0-3.3V. Engine speed is measured using the Hall sensor A3144.

When a magnet on the engine blades approaches the Hall component, it alters the magnetic field, producing a high-level signal. As the engine rotates, the magnet moves away, causing the output signal to become low, generating a pulse signal. The microcontroller receives this pulse signal via a peripheral interrupt and calculates the engine speed accordingly.

4.4 Drive circuit

The drive circuit controls the throttle valve and engine start-stop.The engine start-stop control system uses the speed signal to manage the starting relay and ignition signal. Specifically, a relay is placed in series in the engine's starting circuit.When the energy management system requires the engine to start, the relay is activated, and the engine is powered by the motor. Another relay is placed in series in the ignition circuit.When the energy management system demands the engine to stop, the relay remains activated until the engine speed reaches 0 r/min.

The throttle valve is controlled by a servo motor via a synchronous belt with a 2:1 transmission ratio. This means a 180-degree rotation of the servo motor corresponds to a 90-degree rotation of the throttle valve. The mechanical connection is shown in Figure 5.The throttle valve control system operates by controlling the servo motor's rotation based on vehicle-related signals.

The servo motor is driven by a chip with 7 pairs of NPN Darlington transistors, which can withstand high currents in parallel. This chip acts as a voltage amplifier, making it ideal for this circuit's requirements. The driver chip's circuit connection diagram is shown in Figure 6.

The servo motor is controlled by phase sequence, with the direction of rotation determined by the value of DIR. When DIR=1, the motor rotates forward; when DIR=0, it rotates in reverse.A servo motor with a torque of 15 kg/cm and accuracy of 3us (KST MS3509) is selected for accurate control.The servo motor's motion is controlled by output pulse width using pulse width modulation (PWM). The PWM signal frequency is 50 Hz, and the high-level part of the pulse width (0.5-2.5 ms) corresponds to a 0 to 180-degree rotation of the servo motor.

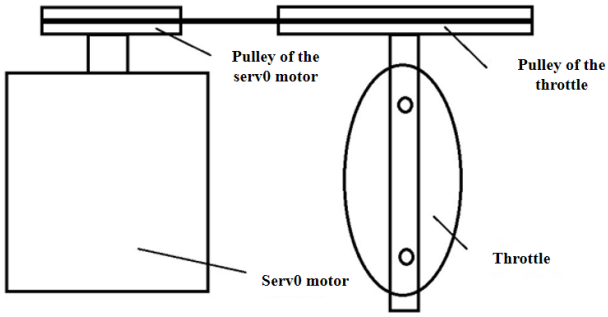

Fig.5 Mechanical connection

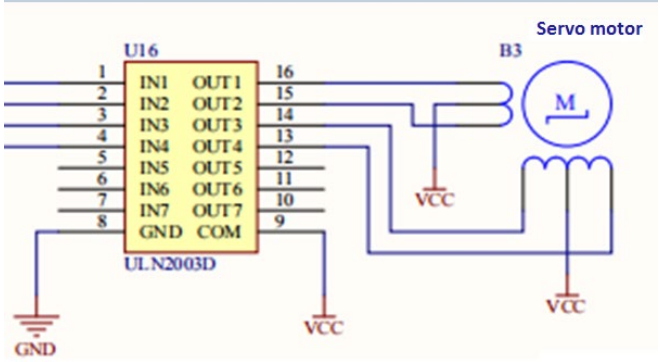

Fig.6 Connection of the servo motor

5. Software design

As mentioned previously, the control system is utilized to regulate the engine's charging of the battery.The Thermostat Control Strategy (TCS) is

employed in the battery management, and the workflow is depicted in Figure 7. The program commences with initialization, which encompasses setting parameters, configuring channels, and establishing sampling rates. The battery's current is continuously monitored, and the SOC value is estimated. If the SOC value is less than 10%, the engine start-stop sub-program is executed. If the engine starts, the program proceeds to collect data. Otherwise, the program terminates. During engine operation, the battery's current is monitored, the SOC value is estimated, and the throttle valve position is adjusted accordingly, executing the throttle valve position adjustment sub-program. If the SOC value exceeds 95%, the engine stops, and the program shifts back to data collection and SOC value estimation.

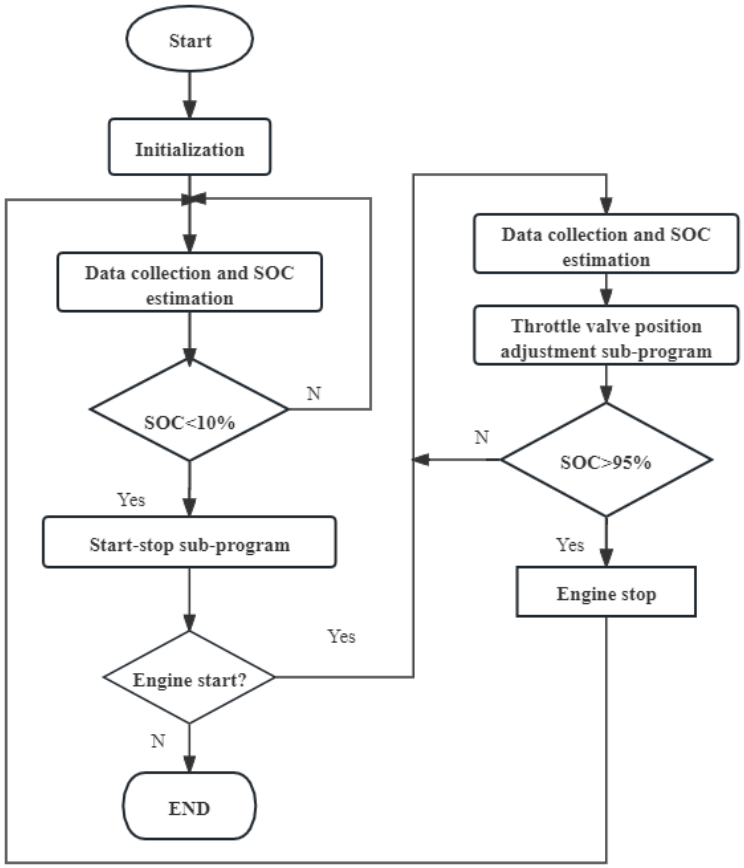

Fig.7 Flow chat of battery energy management

5.1 engine start-stop control

The engine start-stop control sub-program operates based on engine speed. When the start process begins, the engine start relay engages, and the speed sensor signal is calculated. If the engine speed exceeds 200r/min, the relay disengages, and

the engine starts. However, if the engine speed is below 200 r/min and the start process takes less than 10 seconds, the engine continues to start with the relay engaged. If the start process exceeds 10 seconds, the engine start fails, and the flag is turned off. The flow chart is shown in figure 8.

5.2 SOC estimation

SOC estimation is a crucial aspect of the control system, and the ampere-hour integration method is employed in this design. The initial SOC value is calculated by first collecting the open-circuit voltage.Subsequently, SOC is estimated using the ampere-hour method by collecting the battery current.

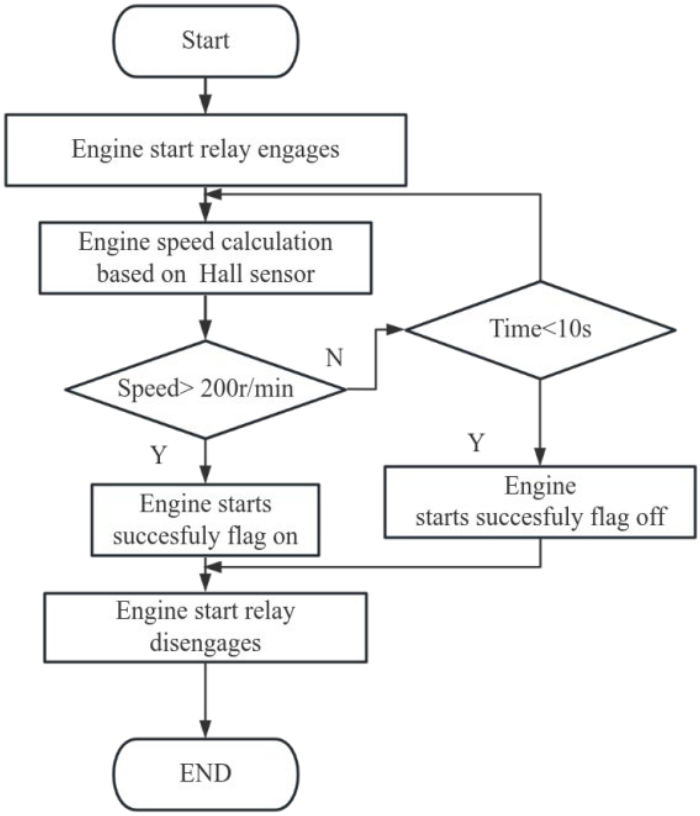

Fig.8 Flow chart of the servo motor control

5.3 Throttle valve position adjustment

For throttle valve position adjustment, the straightforward method is to set the throttle valve at 50% wide open throttle (WOT) regardless of the SOC value. Based on the TCS battery management, a multi-point battery management strategy is presented, and the workflow is illustrated in Figure 9.

There are two distinct standards according to SOC variation. If the SOC is descending, the throttle valve position is adjusted to 50%, 75%, and 100% WOT

when the SOC value is 80%, 50%, and 20%, respectively. If the SOC is increasing, the throttle valve position is changed to 75%, 50%, and 25% WOT when the SOC value is 50%, 75%, and 90%, respectively.

As mentioned previously, the throttle valve is controlled by a servo motor and a throttle valve position sensor. So the closed-loop control is adopted based on the throttle position sensor. The desired throttle valve position is reached by controlling the servo motor's rotation based on the throttle valve position sensor.

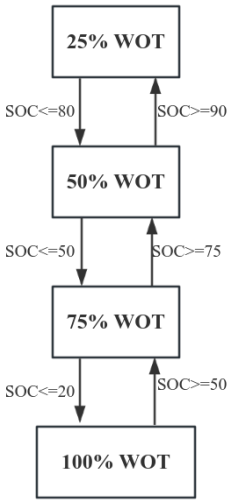

Fig.9 Flow chat of multi-point battery management

Based on the mechanical part selection and control system design, the hybrid vehicle is assembled and the real picture is shown in Figure 10.

Fig.10 Real picture of the modified car

6. Experimental Tests

After assembling the HEV, it was tested on a real road. Initially, the speed, current, and voltage were measured during vehicle operation, and the data are presented in Figure 11. The results indicate that the vehicle operates effectively, and the relevant data can be accurately measured.

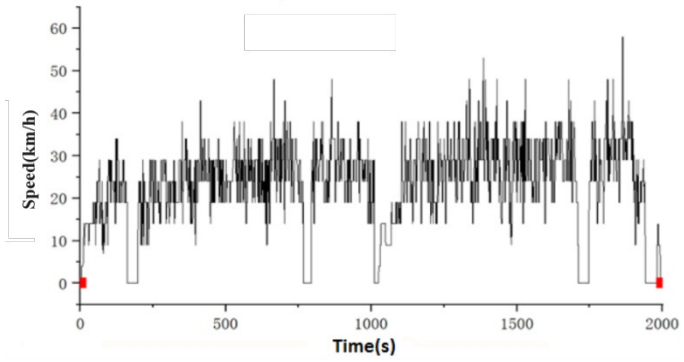

(a) Speed of the vehicle

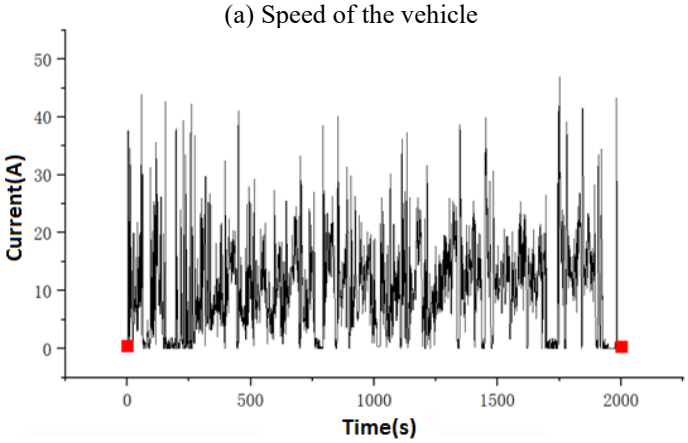

(b) Current of the vehicle motor

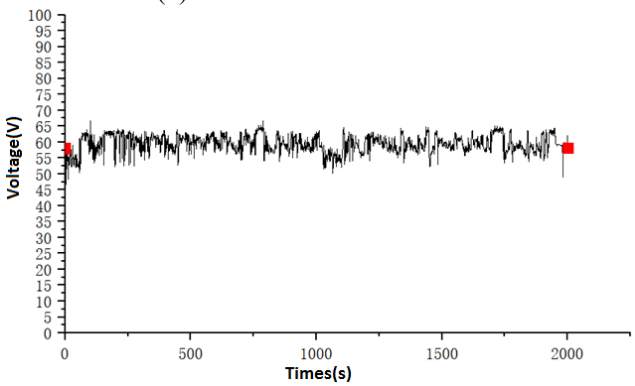

(c) Voltage of the vehicle motor

Fig.11 Experiment results

On a horizontal road, two battery management strategies were tested. Comparisons were made at speeds of 10 km/h, 20 km/h, and 30 km/h. During the experiment, the driving range was set to 4 km, and fuel consumption was calculated based on the mass change of the fuel tank. The test results are presented in Table 3.The results show that the fuel consumption of the vehicle using the multi-point battery management strategy is superior to that of the TCS.

Table3

Comparison of fuel consumption based on different battery management strategy

velocity	Fuel consumption based on TCS	Fuel consumption based on multi-point
10km/h	1.70	1. 50
20km/h	2.00	1.70
30km/h	2.50	2.30

7. Conclusion

Aiming to develop a HEV suitable for experimentation, a hybrid vehicle was designed based on an existing ATV. The design process included selecting the motor, batteries, reducer, throttle valve position control, engine start-stop control, and developing the corresponding program using the STM32F103VET6 microcontroller. Subsequently, the hybrid vehicle was tested on a real road. The experimental results indicate that the vehicle operates normally and meets the anticipated design objectives, facilitating further research on hybrid vehicle performance. Additionally, two battery management strategies, TCS and Multi-point, were tested. The results demonstrate that the Multi-point strategy is superior in terms of fuel consumption.

REFERENCES

[1]. *X. Qiao, Y. Zhang, W. Yang, and et al.,* "Carbon fibre-reinforced polydicyclopentadiene composites for automobile applications", in Materials Letters,vol. 337,no.1,Apr.2023, pp.1-4

[2]. *S. Bairabathina, B. Subramani,* "Design, prototype validation, and reliability analysis of a multi‐input DC/DC converter for grid-independent hybrid electric vehicles", in International Journal of Circuit Theory and Applications, **vol.** 51, no. 5, Apr. 2023,pp.2375-2405

[3]. *Z. Liu , S. Cheng , J. Liu, and et al,* "A Novel Braking Control Strategy for Hybrid Electric Buses Based on Vehicle Mass and Road Slope Estimation", in Chinese Journal of Mechanical Engineering ,**vol.** 35,no.6,Jun.2022, pp.150-150

[4]. *S. Dong, H. Chen, L. Guo, and et al,* "Real-time energy-efficient anticipative driving control of connected and automated hybrid electric vehicles",in Control Theory and Technology, **vol.** 20,no.2,Feb.2022, pp.210-220

[5]. *H. W. Won, A. Bouet,"*Toward the European 2030 CO2 target with gasoline compression ignition technology and 48 V mild electric hybrid",in International journal of engine research, **vol.** 24,no.3,Mar.2023, pp.1190-1199.

[7]. *Y. Yang, J. F. Huang, D. T. Qin,and et al,* "Coordinated Torque Control for Mode-Switch between Motor and Engine Driving in Heavy Hybrid Electric Vehicle", inInternational Conference on Power Transmission.2011

[8]. *N. B. Halima, N.B. Hadj, M. Chaieb,and et al,* "Energy Management of Parallel Hybrid Electric Vehicle Based on Fuzzy Logic Control Strategies", in Journal of circuits, systems and computers, **vol.** 32,no.1,Jan.2023, pp.1.1-1.31

[9]. *Z. Amjadi , S. S. Williamson,* "Prototype Design and Controller Implementation for a Battery-Ultra-capacitor Hybrid Electric Vehicle Energy Storage System", in IEEE Transactions on Smart Grid, **vol.** 3,no.1,Jan.2012, pp.332-340

[10]. *G. Du, Y. Zou, X. Zhang, and et al,* "Heuristic Energy Management Strategy of Hybrid Electric Vehicle Based on Deep Reinforcement Learning With Accelerated Gradient Optimization", in IEEE transactions on transportation electrification,**vol.** 7,no.4,Apr.2021, pp.2194-2208

[11]. *N. Yang, L. Han, R. Liu, and et al,*"Multiobjective Intelligent Energy Management for Hybrid Electric Vehicles Based on Multi-agent Reinforcement Learning", in IEEE Transactions on Transportation Electrification, **vol.** 9, no.3, Sept. 2023, pp. 4294-4305

[12]. *Y.Wang, Y.K. Wu, Y. J. Tang, and et al,* "Cooperative energy management and eco-driving of plug-in hybrid electric vehicle via multi-agent reinforcement learning", in Applied Energy,**vol.** 332, no.2, Feb. 2023, pp.120563.1-120563.12

[13]. *X.L. Sun, J.Q. Fu, H.Y. Yang, and et al,* "An energy management strategy for plug-in hybrid electric vehicles based on deep learning and improved model predictive control", in Energy,**vol.** 265, no.4, Apr. 2023, pp.126772.1-126772.12

[14]. *J. Li, Y.G. Liu, Y.J. Zhang, and et al,* "Data-driven based eco-driving control for plug-in hybrid electric vehicles", in Journal of Power Sources,**vol.** 498 no.1, Jun. 2021, pp.229916.1-229916.12

[15]. *Z.S. Yu,* Automobile theory.Tsing hua press, 2021

[16]. *R. Rajamani.* Vehicle Dynamics and Control. Springer,2006

[17]. *X. Tang, J. Chen, H. Pu, and et al.* "Double Deep Reinforcement Learning-Based Energy Management for a Parallel Hybrid Electric Vehicle With Engine Start–Stop Strategy", in IEEE Transactions on Transportation Electrification, **vol.** 8, no.1, Mar. 2022, pp. 1376-1388